Energy dependence of the optical matrix element in hydrogenated amorphous and crystalline silicon

W. B. Jackson, S. M. Kelso, C. C. Tsai, J. W. Allen , and S.-J. Oh
Xerox Palo Alto Research Center, Palo Alto, California 94304
(Received 5 November 1984)

The energy dependence of the average optical matrix element for both hydrogenated amorphous (*a*-Si:H) and crystalline silicon (*c*-Si) has been determined experimentally, with use of the density of states and the imaginary part of the dielectric function. The valence- and conduction-band density of states of *a*-Si:H and *c*-Si were measured with use of x-ray photoemission and inverse x-ray photoemission spectroscopy, respectively. Using the sub-band-gap density of states measured by isothermal capacitance transient spectroscopy, a nearly complete experimental density of states for *a*-Si:H has been determined. The imaginary part of the dielectric function was measured with use of ellipsometry and photothermal deflection spectroscopy. We find that the average dipole matrix element squared for *a*-Si:H is constant up to ~ 3.4 eV with a magnitude of ~ 10 Å^2 and decreases as E^{-5} at higher energies, where E is the photon energy. The energy dependence of the matrix element is the same as that calculated for complex forms of crystalline silicon (T-12). The matrix element does not depend on the localization of the initial state if the final state is delocalized, indicating that the random-phase approximation is valid for *a*-Si:H. The average dipole matrix element for *c*-Si, determined in a similar manner as *a*-Si:H, has three peaks at 3.4, 4.3, and 5.3 eV. At high photon energies the matrix element falls off as E^{-5}. Finally, it was found that optical determinations of the band gap for *a*-Si:H tend to underestimate the mobility gap.

I. INTRODUCTION

Measurements of optical absorption are widely used to determine characteristics of the electronic density of states (DOS) of hydrogenated amorphous silicon (*a*-Si:H). One of the most common uses of optical absorption is to determine the band gap of the material as a function of various deposition conditions and annealing procedures.[1] The optical absorption has also been used to determine the sub-band-gap and valence-band-tail density of states.[2] However, the optical absorption depends not only on a convolution of the conduction-band (CB) and valence-band (VB) DOS but also on the optical transition-matrix element. From the optical properties alone, it is not possible to uniquely determine DOS properties without simplifying assumptions about the optical transition-matrix element and the DOS.

In most of the previous experiments utilizing optical measurements, the average momentum matrix element squared, $P^2(E)=|\langle f|P|i\rangle|^2$, is assumed to be independent of the photon energy E, where P is the momentum matrix element and $i(f)$ is the initial- (final-) state wave function. This approximation was first made by Tauc.[3] The band gap, for example, is often determined by the zero intercept of a plot of $(\alpha E)^{1/2}$ versus E (Tauc plot) where α is the absorption coefficient. This plot gives a straight line and the band gap only if $P^2(E)$ is constant *and* if both the CB and VB DOS increase as the square root of the energy from their respective band edges. Deviations from these assumptions can lead to significant changes in the resulting band gap. Despite these assumptions, the Tauc plot is by far the most common means of determining the band gap. Another use of the constant momentum-matrix-element assumption has been to determine the density of states from the optical absorption.[2] However, calculations[4] and measurements presented in this paper show that the momentum matrix element for crystalline silicon (*c*-Si) exhibits a considerable dependence on photon energy. There is little reason to expect that the matrix element would be constant in *a*-Si:H either. Thus, it is important to experimentally determine the energy dependence of the optical transition-matrix element.

A number of attempts have been made to investigate the optical properties for amorphous silicon using more realistic models for the matrix element The simplest assumption is that the energy dependence of the optical matrix element is similar to that of *c*-Si. In fact, it has been suggested that the configurational average of $P^2(E)$ for *a*-Si is similar to that of *c*-Si for energies above the direct gap for silicon ($E>3.35$ eV) under the assumptions that the dominant absorption comes from localized valence- and conduction-band states centered on the same site.[5–7] Because of the disorder, any structure due to long-range order such as umklapp enhancements may be expected to be broadened or nonexistent.[5] The high energy dependence was confirmed using x-ray photoemission spectroscopy (XPS) data and Kramers-Kronig reflection data and assuming a step function for the conduction band.[8] Thus, the first estimate was that the matrix element is a smoothed version of the matrix element of *c*-Si with the umklapp enhancements removed.[5,6]

However, the matrix element is quite sensitive to the symmetry of the wave functions. The matrix element for

a-Si:H is expected to be quite different from that of c-Si, particularly below the direct gap where the transition-matrix element of c-Si is zero due to $\mathbf{k}$ conservation. This fact led Paul *et al.* to estimate the matrix element below ~ 4 eV by linearly extending the smoothed crystalline matrix element to lower energy.[5,6] Although this matrix element was estimated for both hydrogenated and unhydrogenated amorphous germanium, the energy dependence may be expected to be similar to a-Si:H other than a shift of the band gap. As pointed out in Ref. 5, this extension of the momentum matrix element was completely *ad hoc* with no physical justification given. This extension results in a matrix element which is largest for transitions near or below the mobility edge and smaller for higher energies.

Later, Cody *et al.*[9] pointed out that although the momentum matrix element is often assumed to be independent of energy, one could equally assume that the dipole matrix element squared, $R^2(E)$, was constant instead. $R^2(E)$ is proportional to $|\langle f|r|i\rangle|^2$ where r is the position. When such an assumption is made, the anomalous dependence of the band gap on film thickness, determined by the assumption of square-root band edges, was eliminated. Klazes *et al.*,[10] on the other hand, claimed that the thickness dependence of the band gap using a Tauc plot could be removed by using a constant $P^2(E)$ but assuming band-edge DOS that varied linearly with energy from the band edges.

In the above-mentioned work, the primary difficulty is that the energy dependence of the matrix element and/or the density of states had to be assumed. Consequently, any conclusions regarding the matrix element or the density of states depended completely on the validity of these assumptions.

Recently, an important step was taken by Ley who used x-ray photoemission data for the valence-band DOS and assumed a broadened step function for the conduction band to determine the joint density of states. By comparing the joint DOS to published optical data,[11] an estimation of the energy dependence of $P^2(E)$ was determined.[12] The estimated $P^2(E)$ exhibited a peak near the direct gap of silicon and decreased for lower energies. However, the behavior of the matrix element below 3.5 eV is very sensitive to the assumed shape of the conduction-band edge, and the DOS and optical measurements were performed on *unhydrogenated* amorphous silicon samples produced under different conditions. The properties of unhydrogenated a-Si vary considerably depending on the method of preparation.

In this paper, we determine the energy dependence of the optical matrix element in both a-Si:H and c-Si without making any assumptions concerning the energy dependence of the conduction- or valence-band DOS. The VB DOS and CB DOS were determined on the same sample by XPS and bremstrahlung isochromat spectroscopy (BIS), respectively. Because the CB DOS could be determined directly, no assumptions about the CB edge were necessary. The optical absorption of a-Si:H from 1.8 to 5.9 eV was measured by ellipsometry on identical films. There was no possibility for spurious effects caused by sample variations. Hence, the energy dependence of the matrix element below the direct gap is determined directly in the region which determines the validity of the Tauc plot.

The energy dependence of the matrix element for a-Si:H was also determined for sub-band-gap energies down to ~ 0.6 eV where the transitions are from localized to extended states. The sub-band-gap density of states was determined using isothermal capacitance transient spectroscopy (ICTS). The optical absorption in the sub-band-gap region was determined by photothermal-deflection spectroscopy (PDS) and by the spectral dependence of the photoconductivity (PC) with dc bias light.

We find that the dipole matrix element, $R^2(E)$, is constant within the errors of the experiment for energies up to 3.4 eV and decreases roughly as E^{-5} above this energy. $P^2(E)$ exhibits a peak near the direct gap of crystalline silicon and agrees remarkably well with the calculated energy dependence of complex crystalline forms of silicon[4] and random-network calculations.[13] We find that the dipole matrix element of localized to extended states is nearly the same as for extended to extended transitions. This result implies that the random-phase approximation is valid for the conduction band of a-Si:H.

The discussion of the matrix element in this paper is organized as follows. In Sec. II the formulas for defining and calculating the energy dependence of the average optical matrix elements squared are presented. Experimental details are described briefly in Sec. III. Conversion of the XPS, BIS, and ICTS data into a nearly complete DOS for a-Si:H is described in Sec. IV. Finally, the results are presented and discussed in Sec. V.

II. THEORY

In a discussion of the average optical matrix element, it is important to define the averaging process and present the definitions of the optical matrix elements to avoid confusion. The formulas presented below form the basis of our analysis and define the terms used within the rest of the paper.

In the one-electron picture using linear-response theory, the imaginary part of the dielectric function, ϵ_2, is given by[12]

$$\epsilon_2(E)=\left[\frac{2\pi e\hbar}{mE}\right]^2\frac{2}{V}\sum_{v,c}|\boldsymbol{\eta}\cdot\mathbf{P}_{v,c}|^2\delta(E_c-E_v-E)\,, \tag{1}$$

where e is the electron charge, m is the electron mass, V is the illuminated volume, $\boldsymbol{\eta}$ is the polarization vector of the incident light, E is the photon energy, and E_v (E_c) is the energy of the initial (final) state. $\mathbf{P}_{v,c}$ is given by $\mathbf{P}_{v,c}=\langle c|\mathbf{P}|v\rangle$, where $\mathbf{P}$ is the momentum operator, $|v\rangle$ is a valence-band state, and $|c\rangle$ is a conduction-band state. In Eq. (1) the summation is over all the single-spin states of the valence and conduction bands which are assumed to be occupied and unoccupied, respectively. The number of single-spin states of the valence band is $2\rho_A V$, where ρ_A is approximately the atomic density of c-Si. The factor of 2 occurs because each spin subband has absorption from the valence to conduction band. Since there are two sets of spin sub-bands and spin flips are not allowed, the absorption is increased by a factor of 2.

From commutator relations one obtains

$$\sum |\boldsymbol{\eta}\cdot\mathbf{P}_{v,c}|^2\delta(E_c-E_v-E) = (mE/\hbar^2)^2\sum |\boldsymbol{\eta}\cdot\mathbf{R}_{v,c}|^2\delta(E_c-E_v-E)\ , \quad (2)$$

where $\mathbf{R}_{v,c}=\langle c|\mathbf{r}|v\rangle$ is the dipole matrix element and $\mathbf{r}$ is the position. In addition, for amorphous materials and unpolarized light, the directional average of $|\boldsymbol{\eta}\cdot\mathbf{R}_{v,c}|^2$ yields $\frac{1}{3}R_{v,c}^2$ where $R_{v,c}$ is the amplitude of the dipole matrix element. The result is

$$\epsilon_2(E)=(2\pi e)^2\frac{2}{3V}\sum_{v,c}|R_{v,c}|^2\delta(E_c-E_v-E)\ . \quad (3)$$

Equation (3) may be written in the form

$$\epsilon_2(E)=(2\pi e)^2\frac{2}{3V}[R'(E)]^2\sum_{v,c}\delta(E_c-E_v-E)\ , \quad (4)$$

where

$$[R'(E)]^2=\frac{\sum_{v,c}\delta(E_c-E_v-E)|R_{v,c}|^2}{\sum_{v,c}\delta(E_c-E_v-E)} \quad (5)$$

is the dipole matrix element squared averaged over all transitions separated by the energy E. The sum in the denominator of Eq. (5) is just the number of states separated by E and can be rewritten in terms of the total valence- and conduction-band DOS, $N_v(E)$ and $N_c(E)$, respectively. We obtain the relation

$$J(E)=4/V^2\sum_{v,c}\delta(E_c-E_v-E) = \int N_v(E')N_c(E'+E)dE'\ , \quad (6)$$

where the factor of 4 comes from the fact that the left-hand side is summed over single-spin states, while $N_v(E)$ and $N_c(E)$ are total DOS including both spin orientations. $J(E)$ is the joint density of states.

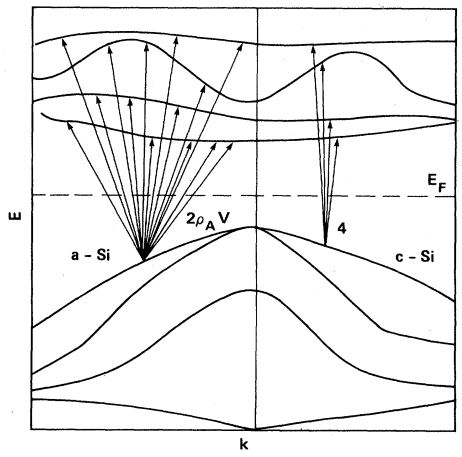

FIG. 1. Nonzero optical matrix elements for a-Si:H and c-Si from a particular valence-band state. Since there is no $\mathbf{k}$ conservation in a-Si:H, all transitions are allowed.

The average used to define $[R'(E)]^2$ is over all states regardless of whether $\mathbf{k}$ is conserved or not. An alternative average used in the case of crystals where $\mathbf{k}$ is a good quantum number is to average just over the transitions conserving $\mathbf{k}$. This average will be significantly larger than the non-$\mathbf{k}$-conserving average. If Eq. (5) is used for c-Si, most of the matrix elements in the sum are zero because of $\mathbf{k}$ conservation. In particular, if the diagram in Fig. 1 is considered, only four of the transitions from a possible $2\rho_A V$ transitions are nonzero. Thus, we would expect the average matrix element squared defined by Eq. (5) to be smaller than the matrix element averaged over $\mathbf{k}$ allowed transitions by a factor of $\rho_A V/2$. Let us define a normalized average matrix element $R^2(E)$ by the relation

$$R^2(E)=[R'(E)]^2\rho_A V/2\ . \quad (7)$$

This average matrix element squared may be used to directly compare the non-$\mathbf{k}$-conserving average of c-Si with a-Si:H and with c-Si band-structure calculations which utilize a $\mathbf{k}$-conserving average. Or in other words, a single matrix element for an individual transition in a-Si:H is roughly $\rho_A V/2$ times smaller than an allowed matrix element for c-Si but the non-$\mathbf{k}$-conserving average, $[R'(E)]^2$, is of the same order of magnitude in both. $R^2(E)$ is also of the same order of magnitude in both c-Si and a-Si:H but is much larger since it is of the same order of magnitude as the $\mathbf{k}$-conserving average and thus can be used to compare to theory.

Substituting Eqs. (6) and (7) into Eq. (4), the following relationship is obtained:

$$\epsilon_2(E)=(2\pi\epsilon)^2R^2(E)/(3\rho_A)\int N_v(E')N_c(E'+E)dE' =0.43\times10^{-44}R^2(E)J(E)\ , \quad (8)$$

where $J(E)$ is in states^2 eV^{-1}cm^{-6} and $R^2(E)$ is in units of Å^2. The average momentum matrix element squared can be obtained from Eqs. (2) and (8):

$$P^2(E)=m^2E^2R^2(E)/\hbar^4=1.68\times10^{-2}E^2R^2(E)\ , \quad (9)$$

where E is in units of eV and $P^2(E)$ is in units of Å^{-2}.

The matrix elements defined in Eqs. (8) and (9) may be compared in magnitude to those calculated in Refs. 4 and 14—16. Recently, some authors have introduced a more general average matrix element, $M(E_v,E_c)$, which depends not only on the photon energy but also on the initial state.[14,17,18] While from a theoretical point of view there is more information in such an average matrix element, it is not an experimentally accessible quantity since one is unable to determine the absorption due to a single valence-band state. Because experiments are confined to measuring averages over the initial state, this average matrix element cannot be used to test the various conjectured energy dependences mentioned in Sec. I.

We have neglected many-electron effects in the above equations for ϵ_2. This should not be important for a-Si:H since it is expected that the exciton binding energies are less than the disorder energy of the material. Consequently, the excitonic enhancements should be broadened out and no sharp structures should be apparent. For c-Si, one might expect some significant exciton enhancements of

the matrix element derived using Eqs. (8) and (9), particularly near the band edges.

III. EXPERIMENTAL METHODS

A. Material preparation

Films of a-Si:H were prepared in an ultrahigh-vacuum (UHV) system with a base pressure of $(0.5-2)\times10^{-8}$ Torr (Ref. 19). All samples were deposited using 2-W rf power and 100% silane onto substrates held at 230 °C. For the XPS and BIS measurements, the 100-nm-thick undoped films were deposited on Mo substrates which are known to prevent substrate-induced crystallization.[20] Two sets of samples were used for the ellipsometry and PDS measurements. One set of samples consisted of 75-nm undoped films deposited concurrently with the XPS samples onto Corning 7059 glass substrates. A second set of 3-μm undoped samples were deposited under identical conditions onto Corning 7059 substrates. The optical properties of the two samples were nearly identical above 1.5 eV. Finally, for the deep-level transient spectroscopy (DLTS) measurements, a set of Schottky barrier samples was prepared consisting of a bottom 100-nm Cr contact followed by a 30-nm n^+ layer. Then a 2-μm layer doped by 10^{-5} $[PH_3]/[SiH_4]$ in the gas phase was deposited followed by 2-mm Pt dots at the top surface. Ellipsometry measurements could be made on these samples since the top electrodes did not cover the entire sample. Further details of the 10^{-5} $[PH_3]/[SiH_4]$ samples used for ICTS measurements are described in Ref. 21. XPS and BIS measurements were also performed on 1 Ω cm P-doped c-Si samples cleaved *in situ*.

B. XPS and BIS measurements

The XPS and BIS measurements were performed using a Vacuum Generators ESCALAB, factory modified for BIS. The base pressure was less than 10^{-10} Torr. The XPS measurements were made using the Al $K\alpha$ line (1486 eV). The BIS measurements of the CB DOS used a photon energy of 1486.6 eV. Since the electron escape depth is 3 nm at these energies, the XPS and BIS spectra are characteristic of the bulk. Further details may be found in Refs. 22 and 23.

One particularly useful feature of the measuring apparatus was that the condition of the sample surface could be monitored using the XPS spectra of the core levels. The ratio of the O($1s$) level to the Si($2p$) core-level intensity was less than 0.03, indicating that the oxidation was less than 0.05 of a monolayer.[12] The a-Si:H completely covered the substrate since no evidence for Mo core levels was found. No evidence for charging was found during either the BIS or XPS measurements. The core levels were sharp and DOS features did not shift upon increase of current.

The resolution function of the BIS and XPS measurements was determined by measurements on Ag near the Fermi level. Since the Fermi function is nearly a step function, the derivative of the Ag spectrum provides an empirical determination of the resolution function. The positions of the Fermi level for the BIS and XPS spectra were determined by measuring spectra of the metal substrate in contact with the sample. The position of maximum slope of the BIS and XPS was taken to be the position of the Fermi level. The accuracy of this method is ±0.1 eV.

Previous work has shown that the XPS- and BIS-derived DOS are not affected by the introduction of 10^{-5} $[PH_3]/[SiH_4]$.[23,24] For example, at least 0.1% B must be incorporated before the BIS spectra exhibit any detectable change. Hence, the XPS- and BIS- derived DOS of the undoped samples can be used for the 10^{-5} $[PH_3]/[SiH_4]$ sample as well. This conclusion is further supported by the optical measurements described below.

The resulting XPS and BIS spectra are shown in Fig. 2 for c-Si and a-Si:H. The curves are positioned so that the Fermi levels for the XPS and BIS spectra occur at the same energy. The energy zero is at the mobility edge. The analysis used to transform these spectra into DOS is discussed in Sec. IV.

C. Ellipsometry measurements

Complex dielectric functions were measured from 1.5 to 5.9 eV using a rotating-polarizer ellipsometer.[25] Spectra were measured for 100-nm- and 2-μm-thick undoped samples and for a 2-μm-thick 10^{-5} $[PH_3]/[SiH_4]$ sample. Natural oxides were not stripped prior to measurement. Only the doped sample was rinsed with methanol (to remove hydrocarbon contaminants) because of the poor adhesion of the undoped films to the glass substrates. All spectra showed interference oscillations at low energies, where the a-Si film becomes transparent, due to reflections from the back of the film. Figure 3(a) shows the imaginary part of the dielectric function, ϵ_2, uncorrected for overlayers, for the thicker undoped sample. This spec-

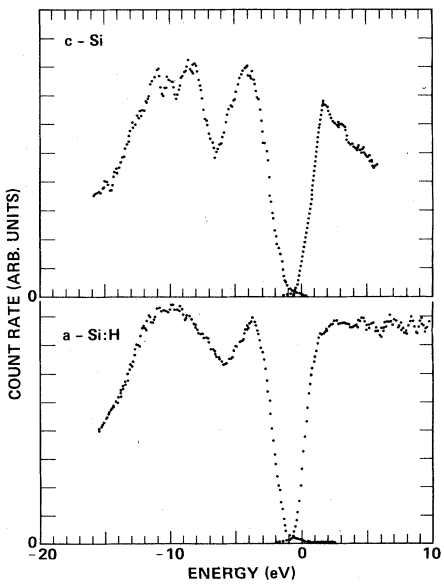

FIG. 2. XPS and BIS spectra for c-Si and a-Si:H. The XPS and BIS spectra are positioned relative to each other as described in the text. The zero is at the conduction-band mobility edge.

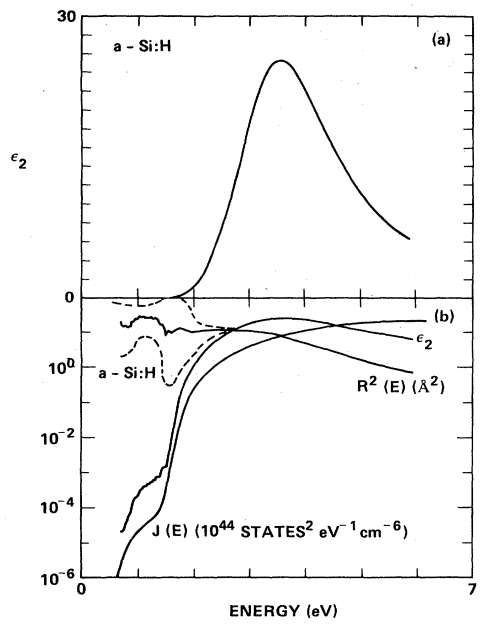

FIG. 3. (a) Linear plot of ϵ_2 versus photon energy; (b) logarithmic plot of ϵ_2 obtained from PC ($E<2.4$ eV) and ellipsometry ($E>2.4$ eV); the joint density of states, $J(E)$, from Eq. (6); and $R^2(E)$ derived using Eqs. (4), (5), and (7). The dashed lines indicate error estimates of one part of the curve relative to other parts. The error on the absolute magnitude is approximately 10%. The large error bars near the exponential edge occur because the small uncertainty about the beginning of the exponential tails translates into a large uncertainty in $R^2(E)$.

trum was used in the subsequent analysis.

Although the dielectric function spectra measured by different groups for undoped unhydrogenated a-Si are very similar,[26] it is known that hydrogenation affects the optical properties. In particular, for low H concentrations the primary effect is a density decrease, while for higher concentrations an additional distortion is observed as the Si—H bonds transfer oscillator strength to higher energies.[27] For this reason, we used optical data for films deposited under the same conditions as the samples used for other measurements.

Some differences were found in the recorded spectra of the three samples. In order to investigate these differences we made quantitative comparisons with reference data for undoped unhydrogenated material.[26] All samples showed bulk density deficits of 4—7%, which is consistent with the amount of H incorporation expected for the deposition conditions. In addition, all spectra had distortions characteristic of a microscopically rough surface layer 15—20 Å thick. The presence of an SiO_2 overlayer was not conclusive except for the doped sample, which had aged for two years to an oxide thickness of ~ 8 Å. We conclude from these comparisons that the bulk optical properties of all three films are very similar. Thus the band gap, DOS, and hydrogen incorporation for the BIS and XPS samples were the same as for the samples used in the ICTS and PC measurements. Changing the sample thickness or introducing light doping does not alter the CB and VB bands significantly.

D. Photoconductivity and PDS measurements

The optical absorption below 2.3 eV was also determined using the spectral dependence of the photoconductivity and PDS in a variety of samples. Since these measurements are described in more detail elsewhere, they will be only briefly summarized here.

The PDS measurements were performed using CCl_4 as the deflection medium.[28] The phase of the signal was monitored to ensure that no absorption occurred in the substrate or deflecting medium. The measurements were made on 10^{-5} $[PH_3]/[SiH_4]$ samples both with and without an n^+ layer. No absorption due to the n^+ layer was found. The PDS absorption agreed within a factor of 2 with that derived using PC for energies above 0.8 eV. Thus, for the analysis, the PC data were used.

The spectral dependence of the ac PC was determined on the same Schottky barrier used in the ICTS measurements. The spectra were taken on the Schottky barrier with 1-V forward bias where the secondary photocurrent dominates. The PC measurements were made using light chopped at 7 Hz and using white dc bias light of ~ 50 times higher intensity. The dc bias light ensured that the quasi-Fermi-levels did not change for different photon energies.[29] Further PC measurements were made on n^+—$n(2\times 10^{-5}$ P)—n^+ sandwich and gap electrode structures to ensure that the PC spectra are accurate measurements of the absorption of the 10^{-5} $[PH_3]/[SiH_4]$ layer.

Using the known film thickness and the saturation of the photocurrent, the absolute absorption coefficient could be determined. The logarithm of the absorption coefficient was arithmetically averaged to remove interference fringes. ϵ_2 was determined from the absorption coefficient and the index of refraction. The index of refraction was estimated by extrapolation of the ellipsometry data and was identical to that found elsewhere for similar samples.[14] The resulting ϵ_2 agreed with the ellipsometry measurements to within 15% over an energy of roughly 0.3 eV near 2.0 eV. The complete ϵ_2 is shown in Fig. 3 combining the ellipsometry and PC data. The error of the sub-band-gap ϵ_2 relative to ϵ_2 above 2.5 eV is conservatively estimated to be less than a factor of 3. The accuracy of ϵ_2 above 2.5 eV is plus or minus a few percent due to variations between samples.

E. ICTS measurements

The ICTS technique for determining gap state DOS is described in Refs. 21, 30, and 31. The ICTS data on the 10^{-5} $[PH_3]/SiH_4]$ samples used in this paper have been reported elsewhere.[21] The optical and PC measurements described in the above paragraphs were performed on the same films used to obtain the ICTS spectra in Ref. 21. The attempt-to-escape frequency, γ, used in the analysis was 10^{-12} sec^{-1}.

IV. TRANSFORMATION OF DATA INTO DOS

In this work, we have attempted to construct an accurate a-Si:H DOS using the best data available from a variety of experimental techniques. In order to increase the accuracy of the DOS, various corrections and checks were applied to the data. These procedures and estimates of the uncertainty are discussed in this section.

A. Valence- and conduction-band densities of states

Several corrections were applied to the BIS and XPS spectra. The inelastic scattering tails and plasmon peaks were removed by a well-known technique described elsewhere using the electron-loss function determined from the valence-band and core-level spectra.[23] The data were then smoothed using a sliding least-squares fit of 15 points. This removes most of the noise due to the Poisson counting statistics.

The effects of instrumental broadening were investigated by a number of different methods. Instrumental broadening can alter the tail region of the density of states and result in an overestimate of the DOS in the gap. These effects will determine the accuracy of the matrix-element calculation in the energy range of 1.5—2.4 eV.

The primary technique was to use a deconvolution routine to determine how much the band edges were affected by broadening. The deconvolution technique used a constrained iterative algorithm and the experimentally determined instrumental broadening function discussed in Sec. III B. The advantages, applications to a number of actual XPS and Auger spectra, and limitations of this algorithm are discussed extensively in Ref. 32. The routine reconstructs the unbroadened spectra starting with the slowly varying components and gradually proceeding to the faster varying components. Since the noise dominates only at the higher frequencies, the procedure may be terminated before the noise becomes important.

The deconvolution procedure is illustrated in Fig. 4. A known edge (solid line) was first broadened by the experimental response function and then noise comparable to that present in the real data was added (points). This known edge has the same slope as the actual data. The deconvolution after ten iterations is shown by the dashed line. The slopes of the solid and dashed curves are nearly identical, indicating that the deconvolution works well.

We applied the same deconvolution procedure to the data. The resulting CB edge is shown in Fig. 5. Since conditions of the deconvolution for the known edge and the actual data are identical, the deconvolved edge of the experimental data is an accurate representation of the DOS.

Another way to test the deconvolution procedure is to deconvolve the c-Si data and compare the results with theory. Figure 6 shows that good agreement is obtained between theory and the deconvolved edge, indicating that the deconvolution procedure is accurate. In particular, the parabolic edge is recovered. The difference in the peak heights is due to the differences in the Si($3s$) and Si($3p$) character which will be discussed below. The deconvolution procedure accurately recovers the DOS.

Finally, the deconvolution procedure and resulting DOS can be tested by convolving the final density of states with the instrumental response and subtracting this convolution from the original data. The residuals (Fig. 7) show that the deconvolved estimates are within the statistical fluctuation of the data.

On the basis of the previously described tests, it can be concluded that the deconvolution provides a reasonable measure of the DOS near the band edges. Therefore, the edges of both the XPS and BIS near the gap were replaced by the deconvolved edges.

The final step in the analysis was to correct for the different cross sections for $3s$ and $3p$ states. Considering the valence band first (Fig. 2), we note that the upper peak is primarily $3p$-like in both c-Si and a-Si:H, while the lower peaks are nearly equal admixtures of s and p.[4] Since the photoionization cross section for the $3s$ states is larger than the $3p$ states by a factor of 3.4, the lower peak is enhanced.[12] Hence, the upper peak was increased by a factor of 1.7 relative to the lower peak. It should be pointed out that this correction only affects the matrix

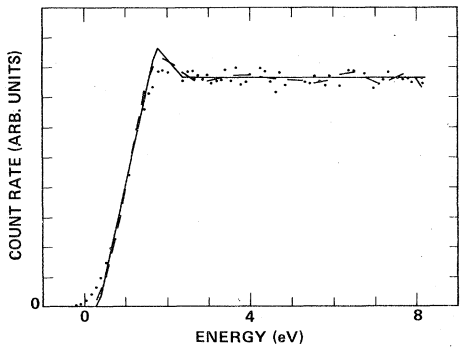

FIG. 4. Test of deconvolution procedure using simulated data. A starting DOS (solid line) was broadened by the instrumental response and Poisson noise was added (points). The point spectrum was deconvolved using ten iterations of the deconvolution routine (dashed).

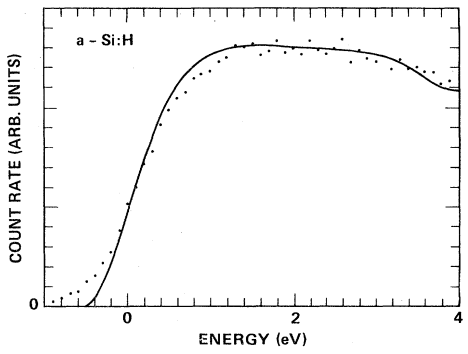

FIG. 5. Actual BIS data for a-Si:H (points). The solid line is the deconvolved curve using the same procedure as in Fig. 4.

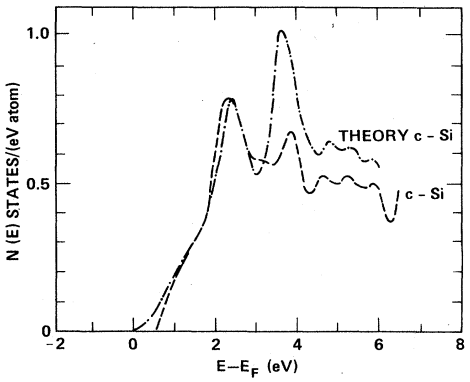

FIG. 6. CB DOS for c-Si. The dashed curve is the deconvolved data of Fig. 2. The theoretical curve is from Ref. 33.

element above 15 eV, outside the range of our optical data.

A similar correction was not made for the CB since these states contain roughly equal admixtures of s and p states. This can be seen from Fig. 6 which shows that the discrepancy between theory and the data for the various critical-point structures of c-Si is much less than the discrepancy in the valence band, indicating roughly equal admixtures of s and p. Since disorder affects the delocalized CB states more than the localized VB states, this approximation is more accurate for a-Si:H. Using the c-Si spectra as a guide, it is estimated that the error in the DOS introduced by this approximation is no more than roughly 10%.

The next step was to determine the magnitude of the DOS for the VB and CB. The normalization of the VB was determined by requiring that the integral number of valence-band states should be equal to four electrons per atom or 17.2×10^{22} states/cm^3. The CB normalization is more involved since there is no clear-cut energy where the $3s$ and $3p$ states end and higher admixtures become important. The magnitude of the a-Si:H relative to the c-Si was determined by taking BIS spectra up to 300 eV above the conduction-band edge. At this energy, the electrons

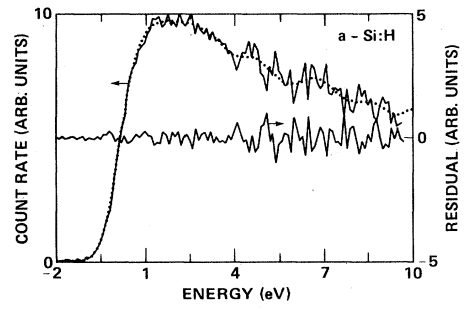

FIG. 7. BIS data (solid curve) are compared with the DOS of Fig. 8 broadened by the instrumental response (points). The difference (residuals) shows that the DOS is consistent with the data. The increase in noise above 4 eV is due to the smaller count time per point.

are nearly free, so the inelastic background and the BIS spectra for the c-Si and a-Si:H should be the same. The amorphous spectrum was normalized at high energies to the crystalline spectrum, while the absolute magnitude of the c-Si DOS was taken from calculations.[33] This procedure is accurate to better than $\sim15\%$.

The conduction- and valence-band DOS were positioned relative to each other by superimposing the Fermi levels of the BIS and XPS spectra. The results are shown in Fig. 8. Since the error in the determination of the Fermi levels from the metal substrate is ±0.1 eV for each spectrum, the energy error of the VB placement with respect to the CB is ±0.15 eV. Because of the rapid decrease of the states towards the gap, this error can be important for the matrix-element determination for energies between 1.5 and 2.0 eV.

At this point in the analysis, we should point out that the corrections made thus far do not significantly affect the shape of the matrix-element—versus—energy curve. In fact, if the raw XPS and BIS data are positioned using the Fermi levels and Eq. (6) is used to determine $J(E)$, the resulting matrix elements are within the error bars of the final results for energies greater than 2.4 eV (discussed in Sec. V).

B. Sub-band-gap density of states

Finally, we discuss the determination of the sub-band-gap DOS. The energy of the DOS obtained from ICTS is measured relative to the conduction-band mobility edge and depends on the value assumed for the attempt-to-escape frequency, γ. In order to place the ICTS states relative to the XPS and BIS DOS, we have determined the position of the Fermi level using the activation energy of the dark conductivity on samples with buried gap electrodes deposited concurrently with the BIS samples. The

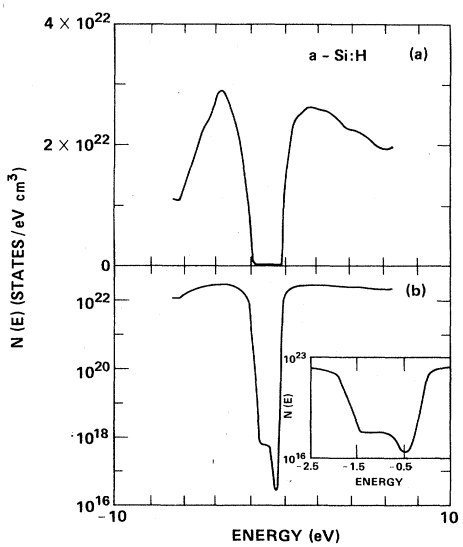

FIG. 8. (a) Linear and (b) logarithmic plots of the complete DOS for a-Si:H. The inset shows an expanded view of the gap DOS.

activation energy observed was 0.82 eV. After correcting for the temperature shift of the gap, we estimate that the CB mobility edge E_c is $\sim 0.87 \pm 0.15$ eV from the Fermi level. The estimated error is due to possible band-bending effects which might effect activation-energy measurements. Knowing the position of E_c, the ICTS peak may be correctly placed within the gap.

There are a number of cross checks which suggest that $N_c(E_c)$ and the ICTS DOS are fairly accurate and consistent with other data. First, from the estimate of E_c we find that $N_c(E_c)$ is between 4×10^{21} and 8×10^{21} states/(eV cm^3). Then the effective number of conduction-band states at room temperature is $N_c kT \simeq 1.5\times10^{20}$ states/cm^3.

Second, we can use this value to estimate γ since $\gamma = N_c(E_c)\langle \nu_{\rm th} \rangle \sigma$ where $\langle \nu_{\rm th} \rangle$ is the thermal velocity and σ is the electron-capture cross section of the neutral dangling bond. From time-of-flight measurements $\sigma \simeq 2\times10^{-15}$ cm^2, yielding $\gamma \simeq 4\times10^{12}$ sec^{-1} (Ref. 34). This value represents a completely independent determination of the value of γ which is very close to that used in deep-level transient spectroscopy[35] and ICTS.[31] This agreement also requires that the energy of the ICTS peak is ~ 0.8–0.9 eV from E_c. Unless the cross-section determination is incorrect by 10^4, we can reject any ICTS energy scales which assume that γ is 10^8 sec^{-1}. The dangling-bond peak must be deeper than 0.4 eV.[36]

Third, if we assume that the valence-band mobility edge, E_v, occurs at the same state density as the conduction-band mobility edge, we find that the mobility gap is ~ 2.0 eV. This value agrees very well with the mobility gap determined by DLTS (Ref. 35) and by luminescence.[37] Fourth, the value of $N_c(E_c)$ is consistent with estimates by Hindley using arguments of Mott[38] and predicts a value of 12 cm^2/(V sec) for the free-carrier mobility within the random-phase approximation. Hence, because the placement of the mobility edge is consistent with many different experiments, the energy scale of the ICTS DOS is probably fairly accurate.

Having placed the ICTS DOS, the DOS is nearly complete except for the band tails and the lower half of the gap. The band tails may be estimated using dispersive transport and optical measurements. In the dispersive-transport theory, the time decay of the current in a time-of-flight measurement is characterized by a parameter $\alpha = T/T_c$ where T is the temperature of the measurement and the density of trapping states has the form $\exp(E/kT_c)$. The optical absorption, on the other hand, has the form $\exp(E/E_0)$. By comparing PDS and dispersive-transport measurements, it is found that there is always close agreement between E_0 and kT_c derived from dispersive-hole transport.[39,40] Hence, although dispersive-transport measurements were not performed on the samples used in the other DOS measurements, the slope, kT_c, of the exponential decay of the valence-band-tail states can be taken from the optical-absorption measurements. The optical measurements yield a value of 52 ± 5 meV for kT_c. The exponential tails of the CB are usually around 26 ± 5 meV as determined from dispersive-transport electrons.[40] Using these data, the band-tail DOS can be estimated.

Unfortunately, the dispersive-transport measurements do not yield measurements of the absolute magnitude of the band-tail DOS and do not extend closer than 0.15 eV to the mobility edge. Consequently, an assumption about the energy at which the exponential tails begin relative to the mobility edges must be made. Although there is one estimate using picosecond absorption that the exponential tail begins within 5 meV of the mobility edge,[41] the results are highly model dependent. Picosecond conductivity measurements[42] indicate that the microscopic mobility at 25 psec is nearly the same as the mobility at 100 nsec, possibly indicating that the DOS is not increasing exponentially near the mobility edge. A recent theoretical treatment suggests that the exponential DOS begins roughly 0.1 eV below (above) the CB (VB) mobility edge.[43] In fact, there is no reason why the exponential region and the mobility edge should coincide. Following Ref. 43, we assume that the exponential band tails begin ~ 0.1 eV within the gap from the mobility edges. The effects of the assumption are discussed in Sec. V.

Finally, our measurements do not provide any reliable information regarding the valence-band region from -1.4 to -1.0 eV. Photoemission total yield[44] and photo-DLTS (Ref. 35) indicate that the density of states is comparable to the magnitude of the dangling-bond peak in this region, often with a second peak appearing 0.4 eV below the dangling-bond level. Consequently, our DOS incorporates a similar shape. Since both the total yield and DLTS exhibit behavior similar to the DOS in Fig. 8, the DOS and, hence, the matrix element, are probably accurate to within a factor of 3 in this region. The complete DOS used in this paper is shown in Fig. 8.

V. RESULTS

In this section the resulting matrix element is determined from the procedures described above for c-Si and a-Si:H. In addition a discussion of exciton effects is presented.

A. Matrix element for c-Si

In order to demonstrate that the measurements and analysis give reasonable results, we first examine crystalline silicon and compare the results to calculations. The valence-band DOS was derived from the XPS spectra as described in the previous section. The data were smoothed, the leading edge into the gap was deconvolved to determine the extent of band tailing into the gap, and the two lower peaks were reduced in magnitude by 1.7 relative to the upper peak. The BIS data were also smoothed and deconvolved. The deconvolved BIS spectrum agrees remarkably well with the calculated DOS, indicating that the deconvolution is accurate (Fig. 6). The data were positioned by lining up the Fermi levels as described above. The final results are presented in Fig. 9.

The ϵ_2 spectrum used was taken from Ref. 45. Using Eq. (8) and the DOS in Fig. 9, $R^2(E)$ was determined (Fig. 10). Also shown is the calculated matrix element for c-Si in the face-centered-cubic or diamond structure (F-2) with two atoms per cell from Ref. 4. The agreement is good considering that (1) the pseudopotential calculation

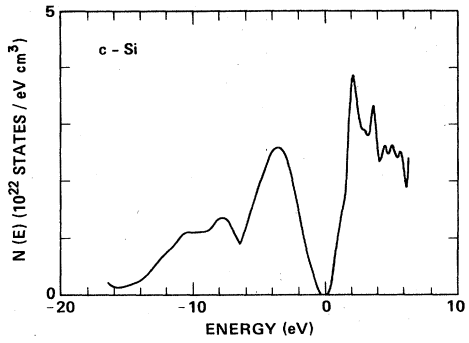

FIG. 9. DOS for c-Si from XPS and BIS data after corrections described in the text.

ignores many-body effects and (2) the average we have determined from the data is over all transitions whereas the calculation is an average over **k**-conserving transitions. The latter approximation is not too extreme near the critical-point energies since the **k**-conserving transitions tend to dominate the non-**k**-conserving joint DOS. Below 3 eV, however, the measured matrix element is small compared with the **k**-conserving average of the theoretical calculations since the transitions are not direct. The two peaks are due to transitions near the L and X points.

Figure 10 also indicates that the magnitude of $R^2(E)$ is roughly 10 Å^2, in agreement with the calculations.[4] Other calculations based on **k**·**p** theory give similar values.[15] Thus, using c-Si as a test case, we see that the data and analysis yield reasonable values of $R^2(E)$. We would expect that $R^2(E)$ for a-Si:H has a similar value.

B. Matrix element for a-Si:H

Having verified our analysis using c-Si, $R^2(E)$ for a-Si:H can be determined. Using the DOS presented in Fig. 8 and Eq. (9), the results in Figs. 3 and 11—13 are obtained. The error bars of $R^2(E)$ are estimated by varying the DOS within the errors of the XPS, BIS, and sub-band-gap measurements. The largest source of error in $R^2(E)$ is due to the uncertainty in the energy at which the

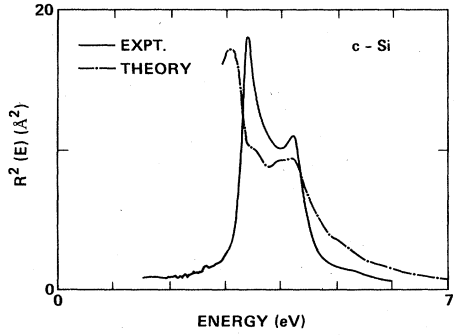

FIG. 10. $R^2(E)$ for c-Si (solid) derived from the DOS in Fig. 6 and ϵ_2. The dotted-dashed curve is the average dipole matrix element for diamond structure c-Si from Ref. 4.

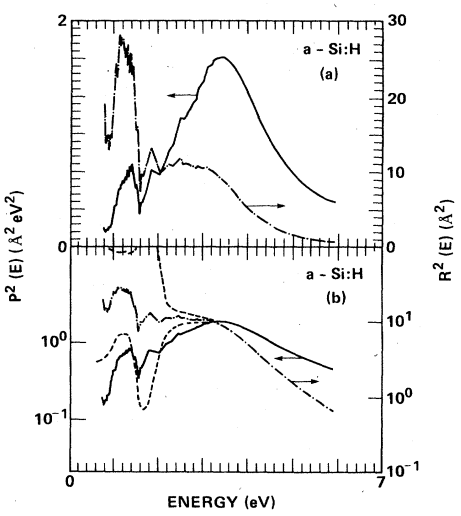

FIG. 11. (a) Linear and (b) logarithmic plots of $R^2(E)$ (dotted-dashed curves) and $P^2(E)$ (solid curves) versus photon energy obtained from the data of Fig. 8(b) and Fig. 3. The dashed curves indicate the error estimates. The large increase of the error bars near 1.5—1.8 eV is due to the rapid decrease in the optical data and the joint DOS at the band edge.

exponential tail states begin relative to the mobility edges. Because the joint DOS and ϵ_2 are changing so rapidly in the (1.5—2.0)-eV region, small changes in the onset of exponential DOS give rise to large changes in the resulting $R^2(E)$ (Fig. 3). The uncertainties in the sub-band-gap region are smaller since $J(E)$ and ϵ_2 vary more slowly. The error in the sub-band-gap region is due to the uncertainty in the absolute value of the defect absorption relative to the above-gap absorption and the uncertainty in the ICTS determination of the sub-band-gap defect density.

$R^2(E)$ is, to within the error of the experiment, independent of energy from 0.6 to 3.0 eV and has a magnitude ($\sim$10 Å^2) very close to that for crystalline silicon. The energy-independent dipole matrix element observed in this study is partially consistent with suggestions that the

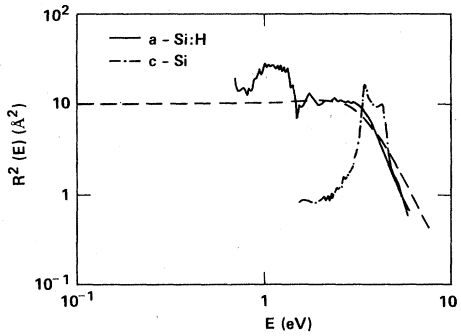

FIG. 12. Log-log plot of $R^2(E)$ vs photon energy (solid). The dotted-dashed curve represents $R^2(E)$ for c-Si. The dashed line is a plot of $1/[(E^2-E_0^2)^2+\Gamma^2E^2]$ with $E_0=3.4$ eV and $\Gamma=4.0$ eV. This is the form of the dipole moment squared for a damped classical harmonic oscillator driven by a field of frequency $\omega=E/\hbar$.

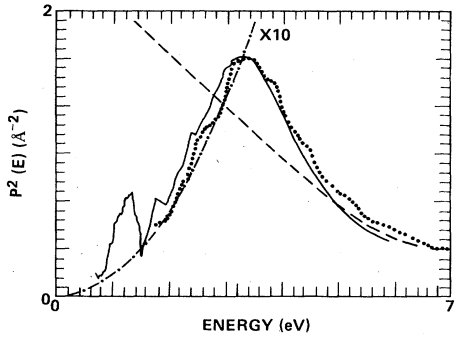

FIG. 13. Comparison of $P^2(E)$ from this paper (solid) to previous results; dashed, Ref. 5; dotted, Ref. 4; dotted-dashed, Ref. 14.

dipole matrix element should be constant and equal to 0.9 Å^2 up to at least 20 eV.[14] The transitions below 1.5 eV are localized to extended transitions while the transitions above 2.0 eV are extended to extended transitions. Thus, the localization of the initial state does not change the magnitude of the matrix element.

The independence of the matrix element on initial-state localization was initially predicted theoretically.[38,43,46] In order for the matrix element to be independent of initial-state localization, the random-phase approximation must hold for the extended CB states. In particular, if the CB state $|c\rangle$ is expanded in terms of states localized on the individual atoms $|n\rangle$, one obtains

$$|c\rangle = \sum_n a_{nc} |n\rangle , \tag{10}$$

where the phase of the complex constants, a_{nc}, must vary randomly from site to site. Thus, our results support the assumption of random phase for the wave function in a-Si:H.

The results are roughly consistent with a simple two-band model (Penn model) of a semiconductor (see Ref. 5 and references therein). We find that $R^2(E)$ falls off roughly as E^{-5} for energies above 3.4 eV, while a decrease as E^{-4} is expected from the Penn model for energies much larger than the band gap.[5,6] Real semiconductors should exhibit this dependence at photon energies larger than the band gap but less than the energy required for transitions from deeper bands since the high-energy photons see only the average separation of the bands and not the details of the band structure. In fact, above 5 eV, the average c-Si and a-Si:H matrix elements in Fig. 12 are nearly identical. The energy dependence of $R^2(E)$ for a-Si:H is similar to that found for a classical harmonic oscillator with resonant energy of 3.4 eV and damping factor $\sim$4 eV (Fig. 12). The direct gap in c-Si is also about 3.4 eV, the maximum in ϵ_2 for a-Si occurs at $\sim$3.6 eV, and the Penn gap is $\sim$3.6 eV. Thus, the optical properties can to first order, be represented by a band gap of energy $\sim$3.4—3.6 eV.

The energy dependence of the a-Si:H matrix element may be qualitatively understood in terms of the crystalline silicon band structure. If a-Si:H is regarded as a "crystal" with a very large unit cell, the indirect X states in the diamond-structure conduction band get folded to the zone center ($\mathbf{k}=0$). The transitions from the valence-band maximum to these states are now direct. The matrix elements of these direct transitions are of comparable magnitude to the matrix element of the direct transitions of diamond structure Si and have $R^2(E)\simeq 10$ Å^2. The matrix element would then be relatively independent of photon energy up to the direct gap energy. At high energies, the photon energy exceeds the energy of many transitions so the matrix element must drop in magnitude to satisfy sum rules. Or in other words, the valence electrons cannot follow the oscillating electric field of the light and hence do not couple as well.

It is interesting to compare the matrix element shown in Fig. 11 with previous predictions. In Fig. 13 the previous conjectures of $P^2(E)$ are plotted along with the results of this work. Our results are a composite of previous conjectures. The prediction that $P^2(E)$ decreases roughly as E^{-2} for high energies is verified.[5] The extrapolation to lower energies, however, was too large. The assumption that $R^2(E)$ is constant is equivalent to an increasing $P^2(E)$. This conjecture is correct for the low energies but leads to unrealistically large values above 3.4 eV. The discrepancy in the magnitude of the matrix elements of this study and Ref. 14 is due to the excessively large matrix elements at high energy of Ref. 14. In order to satisfy the plasmon sum rule, the matrix element at lower energies was underestimated to compensate for the overestimate above 3.4 eV. Since $R^2(E)$ is 10 times larger than the value in Ref. 14, some of the numerical problems are resolved. If our matrix element is averaged over an energy range of 20 eV, the result is approximately 1 Å^2 in agreement with Ref. 14.

Our results are in better agreement with the matrix element determined for a-Si assuming a step function for the conduction band.[12] Up to 3 eV the shapes are similar, but the matrix element in Ref. 12 follows the dotted line above 3 eV. Hence, the peak position of $P^2(E)$ of Ref. 12 is 0.4 eV lower and the decrease at higher energy is less. These differences may have several origins: (1) the assumption of a step function for the CB DOS, (2) the data are for unhydrogenated a-Si, and (3) the DOS and optical data were from different samples.

Our results for $P^2(E)$ agree remarkably well with the momentum matrix element squared calculated for a complex form of silicon with 12 atoms per unit cell called T-12.[4] Although T-12 has long-range order, it has certain types of local disorder that are believed to be present in a-Si:H such as odd-membered rings and bond-angle variations. The calculated matrix element exhibits an asymmetric peak located near 3.4 eV, a roughly linear decrease at low energies and an E^{-5} dependence for $E>4$ eV. The only discrepancy is that the magnitude of $P^2(E)$ of Ref. 4 is a factor of 4 smaller. The overall agreement of the slope of $P^2(E)$ suggests that zone folding, odd-membered rings, and bond-angle variations are sufficient disorder to give rise to the observed optical properties, and that long-range disorder is not necessary for accurate models of a-Si:H. From a theoretical standpoint, our results are very encouraging. The optical transitions averaged over transitions of a super-cell calculation using a large unit cell should accurately yield the experimentally observed optical properties.

TABLE I. Various energy gaps determined from optical measurements.

Extrapolation or gap	DOS E dependence	Matrix element assumed constant	Gap (eV)
$(\epsilon_2)^{1/2}$	$E^{1/2}$	R^2	1.64
$(\epsilon_2)^{1/3}$	E	R^2	1.49
$(E^2\epsilon_2)^{1/2}$	$E^{1/2}$	P^2	1.86
$(E^2\epsilon_2)^{1/3}$	E	P^2	1.55
E_{04}			1.85
E_{03}			1.68

C. Optical band-gap determination

Lastly, we would like to discuss the accuracy of the various methods for extracting a band gap from optical data. Since the DOS is known, the various methods for determining the optical band gap may be compared to the value obtained from the density of states. Most methods assume that either the dipole or the momentum matrix element squared is constant and that the band edges depend either linearly or as the square root of the energy. The band-gap estimate is determined by a linear extrapolation of $(\epsilon_2 E^a)^b$ versus E to zero. Alternatively, one may recognize that a "band-gap" is arbitrary and define the band gap as the energy at which the absorption coefficient α equals 10^3 or 10^4. Several of these methods are summarized in Tables I and II, including the band gaps determined by extrapolating the DOS of this paper. The uncertainties arise from the positioning of the VB and CB relative to each other, and from not knowing where the exponential tails begin relative to the mobility edge.

Several important results are found. First, the extrapolation of the DOS to zero drastically underestimates the mobility band gap, E_g^{μ}. This is not surprising, since the mobility edges must from both theoretical and experimental arguments lie in a relatively large DOS. The Tauc plot gives a good estimate of the band gap E_g^t, defined as the energy difference between the beginning of the exponential tails. The smallest possible value of E_g^t occurs if the exponential tail region begins ~ 0.1 eV from the mobility edge; E_g^t is then 1.75 ± 0.2 eV. If the exponential tails begin at the mobility edge, E_g^t could be as large as the mobility gap of 1.95 eV. The Tauc plot gives the best estimate of E_g^t because the error in the matrix-element assumption compensates the error in the form assumed for the DOS. A plot of $(\epsilon_2)^{1/2}$ gives a smaller gap which is more consistent with a band gap, E_g^{20}, defined as the difference between the energies where the VB and CB DOS have values of 10^{20} states/(eV cm^3).

TABLE II. Various energy gaps determined from DOS measurements.

Method used to determine gap	Gap (eV)
Linear extrapolation of band edges	1.23 ± 0.15
Square-root extrapolation of band edges	1.82 ± 0.15
E_g^{μ} (mobility edge to mobility edge)	1.93 ± 0.2
E_g^t (exponential tail to exponential tail)	1.83 ± 0.25
E_g^{20} [VB 10^{20} states/(eV cm^3) to CB 10^{20} states/(eV cm^3)]	1.61 ± 0.25

The difference in the extrapolated values of linear and square-root edges may also explain, in part, the large core-exciton binding energies recently reported for a-Si:H.[47] It was found that the photoemission band gap, E_g^p, found from linearly extrapolating the VB maximum slope of XPS and the CB maximum slope of core-level absorption spectra was 0.8 eV for a-Si:H. The Tauc-plot optical gap was 1.75 eV. The difference of 0.95 eV was interpreted as the core-exciton binding energy. The Tauc plot assumes square-root band edges, giving a considerably larger band gap (1.82 eV) than a linear extrapolation (1.23 eV) (Table II). If the linear-extrapolated gap obtained by XPS and BIS is compared with E_g^p of Ref. 47, the core-exciton binding energy is estimated to be ~ 0.4 eV. Thus, part of the binding-energy estimate is due to the difference between the linear and parabolic extrapolation of the band edges of the electrical and optical data, respectively.

VI. CONCLUSIONS

In this paper, a number of important new results were discussed. First, the energy dependence of the average matrix element squared was obtained without assumptions regarding the shape of the density of states. The dipole matrix element for a-Si:H is constant below ~ 3.4 eV and has a normalized value of 10 Å^2. The non-$\mathbf{k}$-conserving average dipole matrix element for crystalline silicon exhibits a large peak at the direct gap at 3.35 eV, at 4.2 eV, and a small peak at 5.4 eV. Both a-Si:H and c-Si matrix elements squared decrease roughly as E^{-5} above 3.4 eV. Second, the matrix element for localized to extended transitions is the same as extended to extended transitions, indicating that the random-phase approximation is appropriate for the conduction band. Third, a nearly complete and reasonably accurate DOS that is consistent with many experimental and theoretical results for a-Si:H has been determined. Fourth, the Tauc plot gives the most accurate estimate of the band gap. Fifth, the DOS at the mobility edge has been estimated to be $(4-8) \times 10^{21}$ states/(eV cm^3). These results demonstrate that a combination of electronic and optical techniques can provide important information for the determination of the density of states in amorphous semiconductors.

ACKNOWLEDGMENTS

We would like to thank N. M. Johnson for providing the ICTS data and M. Cardona, G. A. N. Connell, R. M. Martin, M. Stutzmann, and R. A. Street for helpful discussions. This work was supported in part by Solar Energy Research Institute (Boulder, Colorado) Contract No. XB-3-03112-1.

[1]See, for example, J. Tauc, in *Amorphous and Liquid Semiconductors,* edited by J. Tauc (Plenum, London, 1974), Chap. 4; M. H. Brodsky, R. S. Title, K. Weiser, and G. D. Pettit, Phys. Rev. B **1**, 2632 (1970).

[2]See, for example, W. B. Jackson, Solid State Commun. **44**, 477 (1982); R. Crandall, Phys. Rev. Lett. **44**, 749 (1980); G. Moddel, D. A. Anderson, and W. Paul, Phys. Rev. B **22**, 1918 (1980).

[3]J. Tauc, R. Grigorovici, and A. Vancu, Phys. Status Solidi **15**, 627 (1966).

[4]J. D. Joannopoulos and M. L. Cohen, Phys. Rev. B **7**, 2644 (1973).

[5]W. Paul, G. A. N. Connell, and R. J. Temkin, Adv. Phys. **22**, 529 (1973).

[6]G. A. N. Connell, Solid State Commun. **14**, 377 (1974).

[7]K. Maschke and P. Thomas, Phys. Status Solidi **41**, 743 (1970).

[8]R. S. Bauer, in *Tetrahedrally Bonded Amorphous Semiconductors (Yorktown Heights, 1974),* Proceedings of the International Conference on Tetrahedrally Bonded Amorphous Semiconductors, edited by M. H. Brodsky, S. Kirkpatrick, and D. Wearie (AIP, New York, 1974), p. 26.

[9]G. D. Cody, B. G. Brooks, and B. Abeles, Sol. Energy Mater. **4**, 231 (1982).

[10]R. H. Klazes, M. H. L. M. van den Broek, J. Bezemer, and S. Radelaar, Philos. Mag. B **45**, 377 (1982).

[11]D. T. Pierce and W. E. Spicer, Phys. Rev. B **5**, 3017 (1972).

[12]L. Ley, in *The Physics of Hydrogenated Amorphous Silicon II,* edited by J. D. Joannopoulos and G. Lucovsky (Springer, Heidelberg, 1984), p. 61.

[13]W. Y. Ching and C. C. Lin, Phys. Rev. B **18**, 6829 (1978).

[14]G. D. Cody, in *Semiconductors and Semimetals,* edited by J. Pankove (Academic, New York, 1984), Vol. Z1B, p. 11.

[15]M. Cardona, in *Atomic Structure and Properties of Solids* (Academic, New York, 1972); M. Cardona and F. H. Pollak, Phys. Rev. **142**, 530 (1966).

[16]P. Lawaetz, Phys. Rev. B **4**, 3460 (1971).

[17]M. H. Cohen, C. M. Soukoulis, and E. N. Economou, in *Optical Effects in Amorphous Semiconductors (Snowbird, Utah, 1984),* edited by P. C. Taylor and S. G. Bishop (AIP, New York, 1984) (AIP Conference Proceedings No. 120).

[18]S. Abe and Y. Toyazawa, J. Phys. Soc. Jpn. **50**, 2185 (1981).

[19]C. C. Tsai, J. C. Knights, R. A. Lujan, B. Wacker, B. L. Stafford and M. J. Thompson, J. Non-Cryst. Solids **59—60**, 731 (1983).

[20]L. Ley, K. J. Gruntz, and R. L. Johnson, in *Tetrahedrally Bonded Amorphous Semiconductors,* edited by R. A. Street, D. K. Biegelsen, and J. C. Knights (AIP, New York, 1981), p. 161.

[21]N. Johnson and W. B. Jackson, J. Non-Cryst. Solids **68**, 147 (1984).

[22]W. B. Jackson, S.-J. Oh, C. C. Tsai, and J. W. Allen, Phys. Rev. Lett. **53**, 1481 (1984).

[23]W. B. Jackson, S.-J. Oh, C. C. Tsai, and J. W. Allen, in *Optical Effects in Amorphous Semiconductors (Snowbird, Utah, 1984),* Ref. 17.

[24]B. Von Roedern, L. Ley, M. Cardona, and F. W. Smith, Philos. Mag. B **40**, 433 (1979).

[25]The instrument is similar to a rotating-analyzer ellipsometer described in D. E. Aspnes and A. A. Studna, Appl. Optics **14**, 220 (1975); Rev. Sci. Instrum. **49**, 291 (1978).

[26]D. E. Aspnes, A. A. Studna, and E. Kinsbron, Phys. Rev. B **29**, 768 (1984).

[27]D. Ewald, M. Milleville, and G. Weiser, Philos. Mag. B **40**, 291 (1979).

[28]See, for example, N. M. Amer and W. Jackson, in *Semiconductors and Semimetals,* Ref. 14, p. 83.

[29]H. M. Welsch, W. Fuhs, K. H. Greeb, and H. Mell, J. Phys. (Paris) Colloq. **42**, C4-567 (1981).

[30]H. Okushi, Y. Tokumaru, S. Yamasaki, H. Oheda, and K. Tanaka, Jpn. J. Appl. Phys. **20**, L549 (1981).

[31]N. M. Johnson, Appl. Phys. Lett. **42**, 981 (1983).

[32]R. W. Schafer, R. M. Mersereau, and M. A. Richards, Proc. IEEE **69**, 432 (1981).

[33]J. R. Chelikowsky and M. L. Cohen, Phys. Rev. B **14**, 556 (1976).

[34]R. Street, Philos. Mag. B **49**, L15 (1984).

[35]D. V. Lang, J. D. Cohen, and J. P. Harbison, Phys. Rev. B **25**, 5285 (1982).

[36]H. Okushi, T. Takahama, Y. Tokumaru, S. Yamasaki, H. Oheda, and K. Tanaka, Phys. Rev. B **27**, 5184 (1983).

[37]J. Shah, A. Pinczuk, F. B. Alexander, and B. G. Bagley, Solid State Commun. **42**, 717 (1982).

[38]N. K. Hindley, J. Non-Cryst. Solids **5**, 17 (1970).

[39]D. R. Wake and N. M. Amer, Phys. Rev. B **27**, 2598 (1983).

[40]T. Tiedje, B. Abeles, J. M. Cebulka, and J. Pelz, Appl. Phys. Lett. **42**, 712 (1983); C. B. Roxlo, B. Abeles, C. R. Wronski, G. D. Cody, and T. Tiedje, Solid State Commun. **47**, 985 (1983).

[41]Z. Vardeny, J. Strait, D. Pfost, J. Tauc, and B. Abeles, Phys. Rev. Lett. **48**, 1132 (1982).

[42]A. M. Johnson, D. H. Auston, P. R. Smith, T. C. Bean, J. P. Harbison, and A. C. Adams, Phys. Rev. B **23**, 6816 (1981).

[43]C. M. Soukoulis, M. H. Cohen, and E. N. Economou, Phys. Rev. Lett. **53**, 616 (1984).

[44]S. Griep and L. Ley, in *Proceedings of the Tenth Conference on Amorphous and Liquid Semiconductors,* edited by K. Tanaka and T. Shimizu (North-Holland, Amsterdam, 1983), p. 253.

[45]D. E. Aspnes and A. A. Studna, Phys. Rev. B **27**, 985 (1983).

[46]E. A. Davis and N. F. Mott, Philos. Mag. **22**, 903 (1970).

[47]F. Patella, E. Evangelisti, P. Fiorini, P. Perfetti, C. Quaresima, M. K. Kelly, R. A. Riedel, and G. Margaritondo, in *Optical Effects in Amorphous Semiconductors (Snowbird, Utah, 1984),* Ref. 17.